General Hybrid Multizonal/CFD Approach for Bioreactor Modeling

F. Bezzo, S. Macchietto, and C. C. Pantelides
Centre for Process Systems Engineering, Imperial College of Science, Technology and Medicine, London SW7 2BY, UK

A critical issue in the modeling of aerobic bioreactors is the close interaction between fluid flow and the biological reactions. In particular, shear rate has a large effect on the broth viscosity which, in turn, affects the rate of mass transfer of oxygen from the gas to the liquid phase. We demonstrate how a generic hybrid multizonal/computational fluid dynamics (CFD) modeling approach can be applied to take account of these interactions. The approach to multizonal modeling presented characterizes the flow rates between adjacent zones, and also the fluid mechanical quantities, such as the shear stress, that have important effects on the process behavior within each zone, by means of steady-state CFD calculations. An unstructured model for xanthan gum production in a batch aerobic bioreactor is used for this purpose. The hybrid modeling approach is also applied to structured models involving distributions of cell mass within each zone.

Introduction

One of the key challenges facing process modeling today is the need to describe in a quantitative manner the interactions between mixing, fluid flow, and other phenomena, such as chemical reaction, heterogeneous and homogeneous mass transfer, and phase equilibrium. This is particularly important in the case of complex operations (such as polymerization, crystallization, and biological processes), because it is often these interactions that determine the quality of the product (such as, in terms of the distributions of molecular weights or crystal sizes and shapes). Accurate modeling of such processes is essential both at the design stage (e.g., for equipment design and scale-up without the need for extensive pilot-plant studies) and at the operational stage (such as, for the derivation of optimal control strategies).

Process modeling has made substantial progress over the past years at the level of both individual unit operations and entire plants, and now plays an increasingly central role within most process engineering activities. The latest generation of process modeling software tools is quite flexible, being able to represent a wide range of multicomponent, multiphase and reactive systems. It can also deal with both steady-state and dynamic models subject to discontinuities. It is, however, also true that most of the models used by such tools either ignore all spatial variations of properties within each unit operation (invoking the "well-mixed tank" assumption) or are limited to simple idealized geometries (such as, cylinders with 1- or 2-dimensional property variations). Even in models that represent mass- and heat-transfer phenomena to a high degree of detail, the treatment of fluid mechanics is often quite rudimentary.

Computational fluid dynamics modeling

A more detailed description of fluid mechanics and mixing within process equipment can be achieved via the use of computational fluid dynamics (CFD) technology. This formulates and solves the fundamental mass, momentum, and energy conservation equations in 3-dimensional space (see, for example, Fletcher, 1991, or Ferziger and Peric, 1999). For many processes it is, in principle, possible to incorporate a diverse range of phenomena within these basic equations and/or to complement them by additional conservation equations (such as population balances). Examples of this approach have recently been provided by Wei and Garside (1997), Al-Rashed

Correspondence concerning this article should be addressed to F. Bezzo at this current address: DIPIC-Dipartimento di Principi e Impianti dell'Ingegneria Chimica, University of Padua, via Marzolo 9, I-35131 Padova, Italy.

and Jones (1999), and Baldyga and Orciuch (2001), who studied the incorporation of precipitation phenomena within CFD models.

In practice, however, the applicability of this type of approach is limited, primarily for two reasons:

- The resulting system may be too large to be handled with today's computing technology. This is, for example, the case when CFD models are augmented by population-balance equations (for example, an accurate description of a cell mass distribution may require its discretization over the range of possible cell sizes in terms of tens or hundreds of scalar quantities, which greatly increases both the computational and the memory overhead of the CFD calculation).
- The numerical solution algorithms embedded in CFD tools, which are specifically designed to deal efficiently with the large systems of equations arising from the spatial discretization of the mass, momentum, and energy-conservation equations, cannot cope with the resulting system (see, for instance, Birtigh et al., 2000). This is often the case with non-Newtonian fluids, which are typical in the bioprocessing industry.

Moreover, CFD is currently primarily used for steady-state simulations. Performing realistic dynamic simulations is often problematic due to excessive computational times.

Multizonal models of process equipment

A standard way of describing nonideal mixing within processing equipment is by means of a multizonal representation that divides the equipment volume into a network of interconnected zones. An idealized mixing pattern is assumed for each zone—usually, but not necessarily, corresponding to a perfectly mixed region in space.

Multizonal (or "multicompartment") models have been used in crystallization (Kramer et al., 1999; Bermingham et al., 2000), polymerization (Maggioris et al., 1998, 2000), and bioreactor modeling (Nagy et al., 1995; Vlaev et al., 2000) to describe mixing and other fluid-flow properties as well as complex phenomena, such as crystal and polymer growth, and bioreactions.

As evidenced by the work just described, multizonal models represent a pragmatic trade-off for the modeling of many processes of practical interest. On the one hand, predictive accuracy is greatly improved by taking some account of mixing nonidealities within processing equipment. On the other hand, the increase in computational complexity is relatively modest, typically being only a small multiple of the complexity of models based on idealized mixing descriptions.

However, a fundamental weakness of all multizonal models is the difficulty of characterizing the mass and energy fluxes between adjacent zones. An *a priori* estimate of these may be obtained by means of preliminary CFD calculations based on "representative" physical properties (such as density and viscosity) of the fluid.

Hybrid multizonal/CFD models

Some of the problems inherent in multizonal models can be addressed by hybrid approaches that attempt to combine such models with CFD calculations. One example of such an approach is provided by Bauer and Eigenberger (1999, 2001) in their study of gas–liquid bubble columns. In this case, the multizonal model comprises a number of parallel vertical zones, with 1-dimensional modeling of reaction and mass transfer within each zone. The lateral flows between adjacent vertical zones are computed by a multiphase CFD model. The characteristics of the interactions between gas and liquid (such as the local mean bubble size and the mass flux between liquid and gas) required by the CFD model are, in turn, determined by the multizonal model.

Urban and Liberis (1999) used a hybrid multizonal/CFD modeling approach for the modeling of an industrial crystallization process. In this case, the multizonal model is used to represent both the crystallizer and the ancillary cooling and pumping equipment. Each zone is modeled as a perfectly mixed region and incorporates a detailed description of the crystallization phenomena in terms of a population-balance equation. Both homogeneous and heterogeneous crystal nucleation are taken into account, the latter being a strong function of the turbulent energy dissipation rate. A CFD model of the process, based on a pseudohomogeneous fluid model, is used to determine the directionality and rate of flow between adjacent zones, and the mean energy dissipation rate within each zone. The density and viscosity required by the CFD model are estimated on the basis of the crystal-size distribution determined by the multizonal model.

Bezzo et al. (2000) modeled a dynamic exothermic reactor and temperature control system in terms of a single zone (that is, perfectly mixed tank) model. The latter incorporated a CFD model used to estimate the heat-transfer coefficient estimation between the reactor and the surrounding cooling jacket.

Recently, Bezzo (2002) proposed a general structure for multizonal/CFD modeling. As illustrated in Figure 1, in order to construct a generic multizonal model, the spatial domain of interest is divided into a number of *zones* representing spatial regions in the process equipment. Each single zone, z, is considered to be well mixed and homogeneous. Two zones can interact with each other via an *interface* that connects a *port*, p, of one zone with a port of the other. The flow of material and/or energy across each interface is assumed to be bidirectional (F_p, F_p^{in}, respectively). The transient behavior of a generic zone, z, is described by a set of differential and algebraic equations (DAEs) in time, or a set of integro-partial differential and algebraic equations (IPDAEs) in time, and one or more other nonspatial independent variables (such as particle size).

The multizonal model employs a detailed transient modeling of all relevant physical phenomena, with the exception of fluid-flow ones, over a spatial domain divided into a relatively small number of zones. It can determine the dynamic behavior of the system of interest, provided it is supplied with the mass flow rate for each interzonal interface. In some cases, the phenomena represented in a multizonal model may depend on additional fluid mechanical properties such as the turbulent energy dissipation rate.

The preceding information can be determined by solving a detailed CFD model over the physical domain of the system being modeled. The CFD model focuses solely on fluid-flow prediction, trying to do this as accurately as possible by dividing the space into a relatively large number of cells and solv-

ing only the total mass ("continuity") and momentum conservation equations; thus, the model does not attempt to characterize intensive properties such as composition, temperature, or particle-size distribution. The transient behavior is ignored, based on the assumption that fluid-flow phenomena operate on a much shorter time scale than all other phenomena.

The solution of the CFD model will require knowledge of the distribution of physical properties (viscosity, density, compressibility factor, coefficients for models of non-Newtonian fluids, etc.) throughout the physical domain of interest. These are usually functions of the system-intensive properties and are computed within the multizonal model.

The hybrid model is formed by the coupling of the multizonal model with the CFD model, both representing the same spatial domain. The mapping between the zone and cell descriptions employed by the two models, respectively, is achieved by means of appropriate disaggregation and aggregation procedures (Bezzo, 2002).

Objectives of this article

The experience from the hybrid multizonal/CFD applications described is particularly promising as a realistic way of exploiting the increasing availability of computing power to achieve predictive accuracy beyond that which is attainable using purely multizonal models.

In this article, we will apply the general hybrid multizonal/CFD modeling methodology described earlier to address complex issues in the modeling of batch bioreactor systems. A key phenomenon in many of these systems is the transfer of oxygen from the gas phase to the liquid one. The relevant mass-transfer coefficient is strongly affected by the viscosity of the fluid, which tends to vary significantly both temporally and spatially within the system. It is therefore important for models of such reactors to take account of imperfect mixing.

The lack of suitable physical models and the general complexity of bioreactors are major obstacles to their simulation and other numerical studies. Most models and parameters available in the literature appear to be tailored to describe specific situations: they can often reproduce the observed process behavior within a well-defined scale and regime, but are not appropriate for extrapolation much beyond these limits. Although several simplifying assumptions still have to be made, it will be demonstrated how a hybrid multizonal/CFD modeling may address these problems by accounting for physical phenomena such as mixing and shear-stress effect

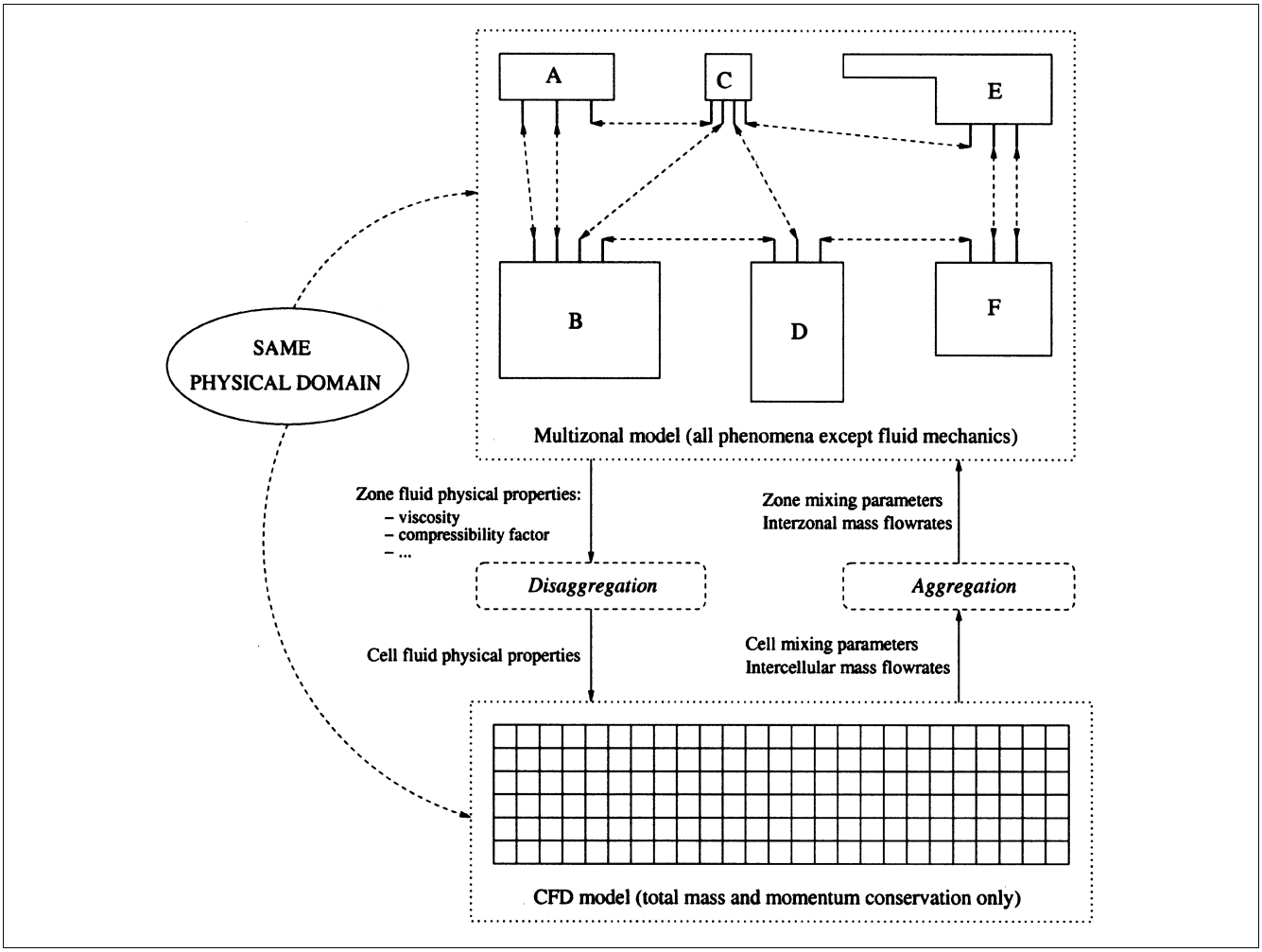

Figure 1. Architecture of the general multizonal/CFD model (Bezzo, 2002).

which, in general, cannot be otherwise represented. The general design of the suggested framework can be applied to different models with minimal changes.

Bioreactor Modeling

Bioreactors represent a wide class of processes of major importance within the process industry. They constitute a typical category of unit operations for which the interactions between hydrodynamics and other phenomena have significant effects on the overall performance. One of the critical parameters in an aerated bioreactor is the mass-transfer coefficient between the gas (air or oxygen) and the liquid (the biological broth) phases, which has an impact on both the yield and growth of microorganisms.

A review of some of the most common general correlations used for the design of such reactors can be found in the book by Atkinson and Mavituna (1991) or in the work concerning non-Newtonian fluids by Badino et al. (2001). Although more correlations may be obtained to model specific systems, there is no effective approach of generalizing these expressions, and consequently uncertainty and inaccuracy remain when scale-up and scale-down are required. For instance, Enfors et al. (2001) consider the complex response to mixing and mass transfer in large-scale bioreactors, and conclude that the use of general correlations cannot predict the process behavior due to the heterogeneity of the system. Nienow (2000) reviews the critical aspects concerning mixing in the manufacture of biological products, showing how tank and impeller design as well as other fluid-dynamic parameters have an impact on biological performance. Hewitt et al. (2000) point out that hydrodynamics may be a critical issue, even at pilot-plant scale, because of shear stress effects. The effect of shear stress on cells is documented in several articles in the literature (such as Papoutsakis, 1991) showing the potential damage to cells (in particular, animal cells) in bioreactors due to agitation and/or aeration. An additional complication arises from the fact that many fermentation fluids exhibit complex rheological properties (Reuss et al., 1982). These heavily affect the mass-transfer coefficient, as demonstrated, for instance, in the work by Li et al. (1995).

The xanthan gum process

We consider a process for the biological production of xanthan gum. Xanthan gum is commercially the most important microbial polysaccharide (Serrano-Carreón et al., 1998). The polymer is produced by cultivation of the bacteria *Xanthomonas campestris*. The success of xanthan gum is due to its very special rheological properties. Xanthan is a water-soluble polysaccharide that has found applications in a variety of industries as a viscosifying, texturizing, and suspending agent. The remarkable stability of the compound over a wide range of salt concentration, temperatures, and pH values also makes it suitable for enhanced oil recovery by polymer flooding (Peters et al., 1989). For this application, high demand for low-cost xanthan is anticipated and, therefore, interest in optimizing the production conditions is growing. The worldwide market is valued at between 600 and 800 million dollars per year, and growing at an annual rate of 6–7% (Cacik et al., 2001).

Batch fermentation is the most common mode for producing xanthan. The fermentation time may vary from 60 h to 120 h, depending on the type of equipment used and the operating strategies. The fermenter is initially charged with a water solution containing the carbon source (glucose or sucrose) and other ingredients (mainly nitrogen). The inoculum with the microorganisms is next injected into the solution. Air (or pure oxygen) is sparged in the vessel while the temperature is maintained within the narrow interval 25–34°C (García-Ochoa et al., 1998). Usually, the pH is set to an initial value of 7.0, but whether or not the pH is controlled during the process is case-dependent (García-Ochoa et al., 1995).

The economics of xanthan production are very dependent on the gum concentration that is attained at the end of the batch (Zhao et al., 1991), and this, in turn, is a function of the precise operating mode (such as batch or fed-batch operations) together with good mixing. The critical factor in this context is the ability to maintain the highly viscous broth in a well-mixed state: variables such as dissolved oxygen and pH are critical, and bad mixing leads to poor control and, therefore, lower yields and/or lower xanthan quality (Serrano-Carreón et al., 1998). The problem is exacerbated by the fact that changes in viscosity during culture exceed four orders of magnitude (Serrano-Carreón et al., 1998). At the beginning of the process, the broth is practically water, but, as xanthan concentration increases, it becomes a very viscous pseudoplastic fluid exhibiting yield stress.

Kinetics of xanthan production

Unstructured models (Bailey and Ollis, 1986) provide the simplest and most commonly adopted approach for modeling microbial systems. They describe microorganisms as an abstract "biomass." Most models of xanthan production are of this type (García-Ochoa et al., 1995; Liakopoulou-Kyriakides et al., 1997; Serrano-Carreón et al., 1998).

Here, we adopt the metabolic kinetic model developed by García-Ochoa et al. (1998). Although the description of microbial growth is carried out by means of an unstructured model, the model is metabolically structured, incorporating a simplified reaction scheme for the intracellular metabolism. We shall return to consider a more detailed "structured" description of the microorganism cells later in this article.

The fermentation reactions are represented by the following set of rate expressions (parameter values are given in Table 1; all other symbols are listed in the Notation section at the end of the article):

- Microbial growth rate

$$r_X = k_X C_X \left(\frac{C_{X_0}}{Y_{XN}} + C_{N_0} \right) \left(1 - \frac{C_X}{C_{X_0} + Y_{XN} C_{N_0}} \right) \qquad (1)$$

- Xanthan gum production

$$r_P = \alpha_3 K C_{O_2} C_X \frac{1 + \alpha_6 k' C_{O_2}}{\alpha_5 + \alpha_6 Y_{ATP,P}} \qquad (2)$$

Table 1. Initial Conditions and Parameters Used in the Xanthan Gum Fermentation Model

Symbol	Description	Value
C_1	Geometry constant	2×10^{-3}
C_{X_0}	Initial biomass concentration ($g\cdot L^{-1}$)	0.053
C_{S_0}	Initial substrate concentration ($g\cdot L^{-1}$)	37
C_{P_0}	Initial xanthan concentration ($g\cdot L^{-1}$)	0
$C_{O_{2,0}}$	Initial dissolved oxygen concentration ($g\cdot L^{-1}$)	2.5×10^{-4}
C_{N_0}	Initial nitrogen concentration ($g\cdot L^{-1}$)	0.25
$C^*_{O_2}$	Equilibrium dissolved oxygen concentration ($g\cdot L^{-1}$)	2.5×10^{-4}
K	Kinetic constant ($g^{-1}h^{-1}$)	79.9
k'	Model constant (mol^{-1})	5.77×10^{4}
k_X	Specific biomass growth rate ($g^{-1}h^{-1}$)	0.535
V_s	Superficial air velocity ($m\cdot s^{-1}$)	1.1×10^{-3}
$Y_{ATP\cdot P}$	Macroscopic yield of ATP into xanthan gum	34
Y_{XN}	Macroscopic yield of nitrogen into biomass	6.073
Y_{XO_2}	Macroscopic yield of oxygen into biomass	239.03
Y_{XS}	Macroscopic yield of substrate into biomass	6.073
α_1	Stoichiometric coefficient	180
α_2	Stoichiometric coefficient	5.94
α_3	Stoichiometric coefficient	923.2
α_4	Stoichiometric coefficient	1/12
α_5	Stoichiometric coefficient	3.58
α_6	Stoichiometric coefficient	4
α_7	Stoichiometric coefficient	0.3
α_8	Stoichiometric coefficient	0.5

Source: García-Ochoa et al., 1998.

- Substrate (carbon source) consumption rate

$$r_S = \alpha_1\left[-\frac{\alpha_2}{\alpha_3}r_P - \alpha_4 K C_{O_2} C_X\left(1-\alpha_5\frac{1+\alpha_6 k' C_{O_2}}{\alpha_5+\alpha_6 Y_{ATP,P}}\right)\right] - \frac{1}{Y_{XO_2}}r_X. \quad (3)$$

- Oxygen consumption

$$r_{O_2} = -\frac{\alpha_7}{\alpha_3}r_P - \alpha_8 K C_{O_2} C_X + k_L a\left(C^*_{O_2} - C_{O_2}\right) - \frac{1}{Y_{OX}}r_X. \quad (4)$$

Equation 1 considers the biomass growth rate to be a function of nitrogen source initial concentration C_{N_0}, but not of the oxygen concentration: García-Ochoa et al. (1995) show that *X. campestris* is not very sensitive to the oxygen mass transfer and can keep on growing even in anaerobic conditions (albeit not for very long). However, if there is not enough dissolved oxygen, xanthan production does not occur.

The other rate expressions are derived from modeling the xanthan production from glucose according to the cell metabolism (ATP cycle; Pons et al., 1989). Correlations can be found to express some of the kinetic parameters as functions of temperature (García-Ochoa et al., 1998). However, in view of the very small heat generation in this process, we consider the system to operate isothermally at 28°C. Additionally, a uniform and constant pH of 7 is assumed.

The mass-transfer model

The mass-transfer coefficient $k_L a$ appearing in the rate expression (Eq. 4) depends on a number of factors, including the effective viscosity of the broth η, the superficial gas (air) velocity, V_s, and the mechanical power input that is a function of the impeller agitation speed, N. All three of these quantities are functions of the hydrodynamics and mixing within the system, either directly or indirectly.

Several correlations for $k_L a$ have been suggested in the literature. Here we adopt the following (see, for example, García-Ochoa et al., 2000; García-Ochoa and Gómez, 1998)

$$k_L a = C_1 V_s^{2/3} N^2 \eta^{-2/3}, \quad (5)$$

where C_1 is a constant (see Table 1).

Thomson and Ollis (1980) describe the evolution of broth rheology by means of a power-law relation for the effective viscosity η

$$\eta = k S^{n-1}, \quad (6)$$

where S is the strain. Values of parameters k and n are estimated from experimental data and appear to be very sensitive to the concentration of polymer in the solution. Recently, Cacik et al. (2001) proposed the following correlations

$$\log k = 0.07327 + 1.49319\log C_P + 0.2763(\log C_P)^2$$
$$n = 0.12865 + 0.4675\exp(-0.5002 C_P) + 0.4156\exp(-7.79 C_P). \quad (7)$$

Serrano-Carréon et al. (1998) developed a more complex model, suggesting the existence of an apparent yield stress τ_0 in the xanthan gum solution at polymer concentrations higher than 10 g/L (Bingham plastic behavior). Apparent yield stress increases with the xanthan concentration. Their model assumes a "concentric boxes" behavior in the reactor. As illustrated in Figure 2, the well-mixed volume or active volume is considered as a region delimited by the apparent yield stress for a given xanthan concentration. The model suggested by Serrano-Carreón et al. takes into account a radius r that determines the volume of the active reactor and that is a function of the effective viscosity. The moving fluid is described by a power-law correlation.

The Hybrid Multizonal/CFD Model

The hybrid multizonal/CFD modeling approach previously described is adopted for the modeling and simulation of xanthan production in a batch reactor of the form shown in Figure 3. The tank is fitted with a double impeller centered shaft and four baffles, and forms part of an existing pilot plant at Imperial College, London (Liu and Macchietto, 1995).

The multizonal model

The multizonal model comprises a network of perfectly mixed internal zones. As has already been mentioned, the system is assumed to be isothermal. Therefore, the dynamic behavior of each zone, z, is primarily described by mass-bal-

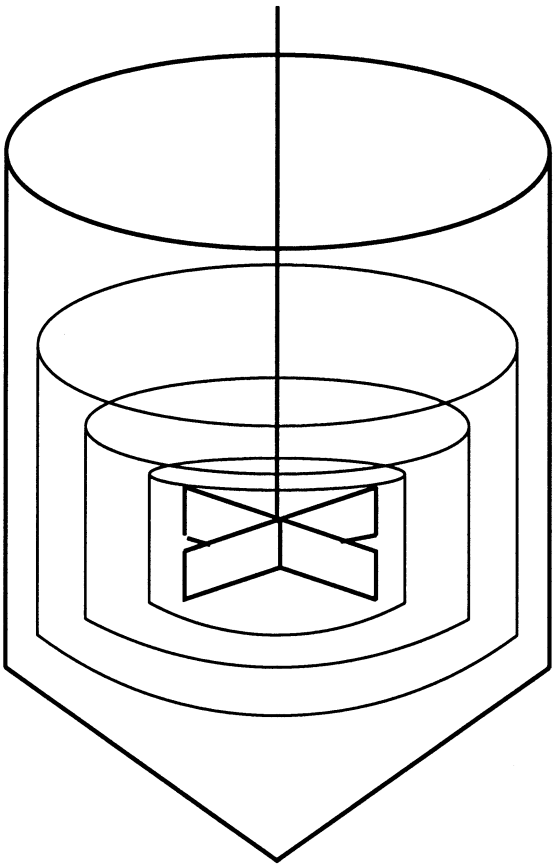

Figure 2. The *concentric boxes* model (Serrano-Correón et al., 1998).

ance equations of the form (in the interests of clarity, we omit the subscript z denoting the zone from the various symbols used in this equation)

$$V\frac{dC_i}{dt} = \frac{1}{\rho}\sum_{p=1}^{np} F_p^{\text{in}} C_{i,p}^{\text{in}} - \frac{1}{\rho}\left(\sum_{p=1}^{np} F_p\right) C_i + Vr_i,$$

$$\forall i \in \{X,S,P,O_2\}, \quad (8)$$

where V is the volume of the zone under consideration; np is the number of ports, p, in the zone; and F_p^{in} and F_p are, respectively, the mass inlet and outlet flow rates associated with port, p. The mass density, ρ, is assumed to be constant ($\rho = 1{,}000$ g/L) and uniform throughout the domain (García-Ochoa and Gómez, 1998).

The reaction rates, r_i, appearing in Eq. 8 are given by Eqs. 1–4, with the mass-transfer coefficient appearing in Eq. 4 being given by Eq. 5.

The mass flow rates between the zones (appearing as F_p and F_p^{in} in Eq. 8) and the effective viscosity within each zone (required by the mass-transfer coefficient of Eq. 5) are computed by the CFD model.

The variation of the gas superficial velocity, V_s (cf. Eq. 5), throughout the fermenter could, in principle, be predicted via a multiphase (gas–liquid) CFD computation. Unfortunately, despite some recent progress in the latter area, most CFD tools that are currently available cannot deal simultaneously with multiphase flow and non-Newtonian liquid behavior of the type described by Eq. 6. Thus, for the purposes of this article, we assume that the superficial air velocity, V_s, is constant and uniform throughout the domain and equal to 1.1×10^{-3} ms^{-1} (García-Ochoa and Gómez, 1998).

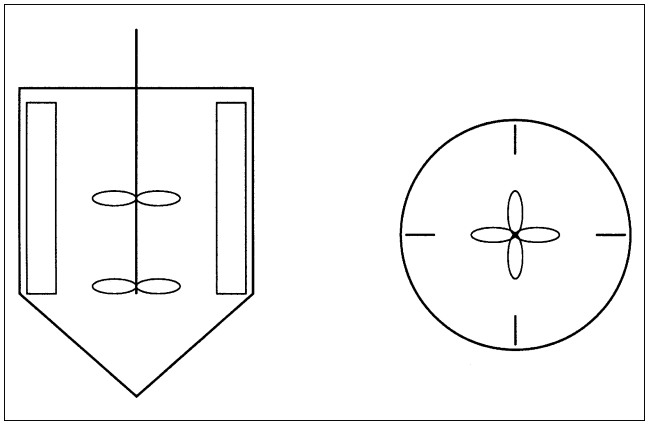

Figure 3. Batch reactor geometry.

The CFD calculation also computes the distribution of the rate of energy dissipation within the vessel. In principle, this could lead to a more precise characterization of the mass-transfer coefficient within each zone. However, no correlations exist for quantifying this effect. We have therefore decided to retain the use of the impeller agitation speed, N, within Eq. 5 as the primary means for describing the dependence of k_La on mechanical power input.

The CFD model

The reactor geometry shown in Figure 3 has two vertical planes of symmetry that are orthogonal to each other. Consequently, only one-quarter of this reactor needs to be represented in the CFD model; the latter involves about 34,000 computational cells organized in a structure grid.

The CFD model solves the steady-state total material and momentum equations. The use of such a steady-state model for the fluid-mechanical phenomena is justified in view of the very long time constants of the fermentation reactions.

The power-law model was adopted for the viscosity, with the coefficients k and n appearing in Eq. 6 being computed by the multizonal model using Eqs. 7. The CFD software (FLUENT, Version 4.5, 1998) used for our computations requires the use of a single set of values for k and n throughout the domain. Consequently, these are obtained by volume-averaging the corresponding values for the individual zones, that is,

$$n = \frac{\sum_z n_z V_z}{\sum_z V_z} \quad \text{and} \quad k = \frac{\sum_z k_z V_z}{\sum_z V_z}. \quad (9)$$

This assumption has little effect on the overall results, since the long time constants of this process tend to minimize local variations in concentration; thus, by far the major cause of

local variations in effective viscosity is the nonuniform distribution of fluid strain.

The CFD model computes the variation of the broth viscosity over its computational grid. The effective viscosity within each zone, z, of the multizonal model is computed by averaging the grid cell viscosities over the zone volume, V_z

$$\eta_z = \frac{\sum_{c \in \mathfrak{C}_z} \eta_c V_c}{V_z}. \tag{10}$$

Multizonal model topology

An important consideration in our hybrid multizonal/CFD modeling approach is the division of the system of interest into an appropriate number of zones, and the topology (that is, connectivity) of the resulting zone network. For the system of interest to this article, the main factor in this context is the variation of broth viscosity over the reactor, and in particular the dependence of η on fluid strain, a quantity that varies widely within the system due to the effects of agitation. The influence of spatial nonuniformities in xanthan concentration on η are less important in view of the long time constants involved. On the other hand, the temporal variation of xanthan concentration does have a significant effect on η.

To investigate the preceding factors, we performed preliminary CFD calculations with uniform values of the k and n coefficients of the power-law model (Eq. 6) being computed using Eqs. 7 at a given uniform xanthan concentration, C_P. Figure 4 shows the velocity and viscosity distributions in the system corresponding to both low and high xanthan concentrations (1 and 10 g/L, respectively). At relatively low xanthan concentrations, the fluid moves throughout the whole domain, although velocity magnitude is greater where viscosity is lower. On the other hand, for high xanthan concentrations, the system starts behaving according to the "concentric box" model proposed by Serrano-Carreón et al. (1998) (cf. Figure 2): flow is effectively restricted to the region close to the impeller; elsewhere the fluid is almost still. Effective viscosity is correspondingly low in the impeller region and much higher near the tank walls.

An interesting conclusion from Figure 4 is that, although the absolute values of the viscosity vary significantly during the batch, it is still possible to subdivide the reactor volume into a number of zones such that, at any particular time, the variation of viscosity within each zone is relatively small. The set of zones was automatically determined by means of an algorithm that allocates the cells in the CFD model into a number of zones such that the variation of each of a given set of properties within each zone is minimized. The algorithm is described in detail in Bezzo (2002). In the case of interest to this article, the set of properties comprised the fluid viscosity at different times during a batch. This has allowed the definition of a fixed multizonal model topology that is valid for the entire duration of the batch.

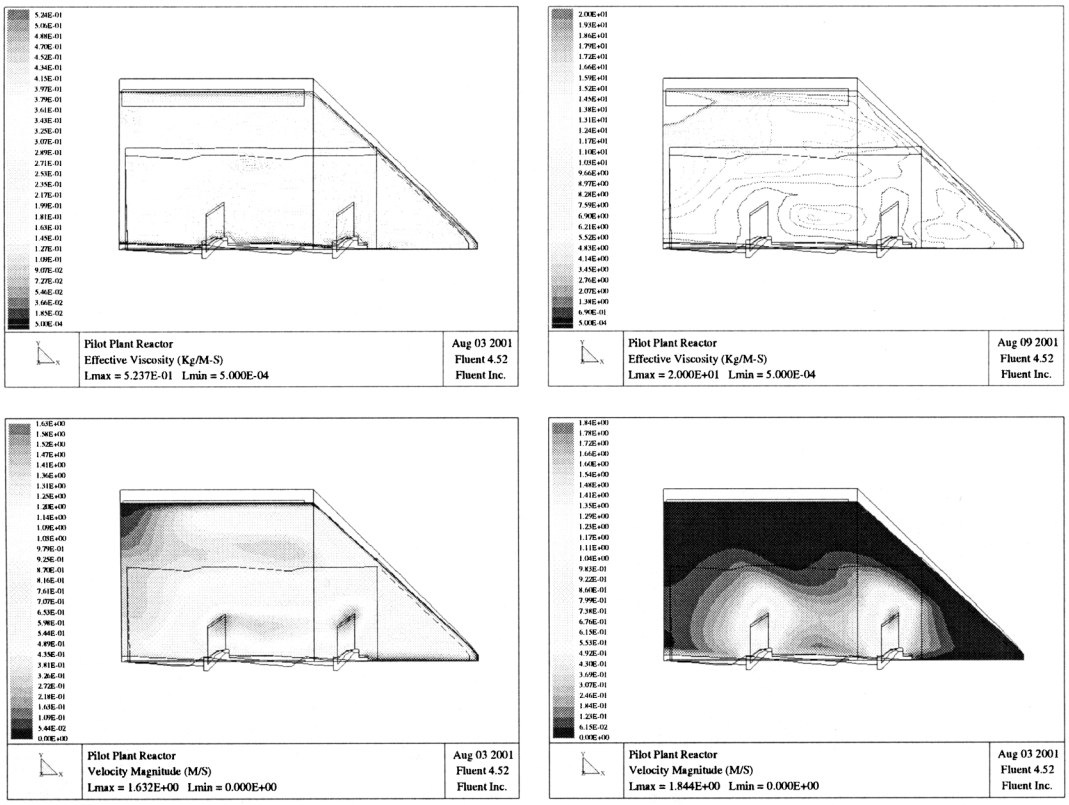

Figure 4. Viscosity (top) and velocity (bottom) distribution at a xanthan concentration equal to 1 g/L (left) and 10 g/L (right).

Software implementation

The multizonal model was implemented in the gPROMS modeling tool (Process Systems Enterprise, 2001). An advantage of gPROMS in the context of the current work is its open architecture, and in particular the gPROMS Foreign Object Interface (Kakhu et al., 1998), which is a general protocol that gPROMS employs for all its communications with external software that may be running on a different computer to that used by gPROMS itself. This is especially important for the purposes of the interface considered here, as CFD software may require the use of specialized hardware.

A general model for a multizonal system has been developed in gPROMS. The multizonal gPROMS model just described has been written in such a way as to be completely independent of the precise nature and behavior of the internal zones in the process under consideration. Instead, it merely expects all valid zone models to expose a certain external interface. Consequently, users wishing to model a new process (such as crystallization, homogeneous reaction, fermentation), or to consider different models for the same process, can do so simply by replacing the implementation of the internal zone models (Bezzo et al., 2003).

The gPROMS package uses an implicit variable-step variable order for the integration of the DAE system describing the multizonal model. In evaluating the residuals of the equations, it invokes the CFD calculation to compute the interzonal flow rates and the average zone viscosities for given values of the parameters n,k. Although the first invocation of the CFD calculation is particularly time-consuming, subsequent calculations are much faster, as they are always started from the solution obtained at the previous call.

Dynamic Simulation of Batch Xanthan Production

The hybrid model described in the previous section is used to simulate the performance of a batch xanthan process over a 50-h period. The first issue that must be addressed in this context is the determination of an appropriate number of zones for the multizonal model. Figure 5a shows the temporal variation of the xanthan gum concentration over the batch, as predicted by hybrid multizonal/CFD models with different numbers of zones. It can be seen that the number of zones does have a significant effect on the predicted concentration of gum in the final product. If the number of zones used is too small, then the variability of the properties of interest within individual zones may not be too large for the well-mixedness assumption to be justified. However, as the number of zones increases, the model predictions approach a limiting solution. For the case shown here, the predictions for 20 and 25 zones are practically identical. Consequently, all of the results presented in the rest of this article have been obtained by a model with 20 zones.

Figure 5b shows the effect of the speed of agitation on xanthan gum production. As expected, the greater the rotation speed, N, of the impeller, the higher the polymer yield, since mass transfer of oxygen from the gas to the liquid phase is a limiting step that is affected both directly (via N) and indirectly (via the dependence of viscosity on fluid strain) by the agitation in the vessel.

The wide temporal and spatial variations taking place in the system of interest are illustrated in Figure 6, which shows the variation of the xanthan gum production rate during the batch within each of the 20 zones. Production rates present significant local variations depending on the local viscosity. At the beginning of the batch, most zones demonstrate a substantial increase of the rate due to the growing biomass; however, some zones near the periphery of the reactor stop being productive soon afterwards. After about 10 h, the increasing viscosity causes the rate to drop dramatically throughout the domain, except in those zones immediately surrounding the impeller. This effect is even more evident at high agitation speed, as can be seen by comparing Figures 6a and 6b.

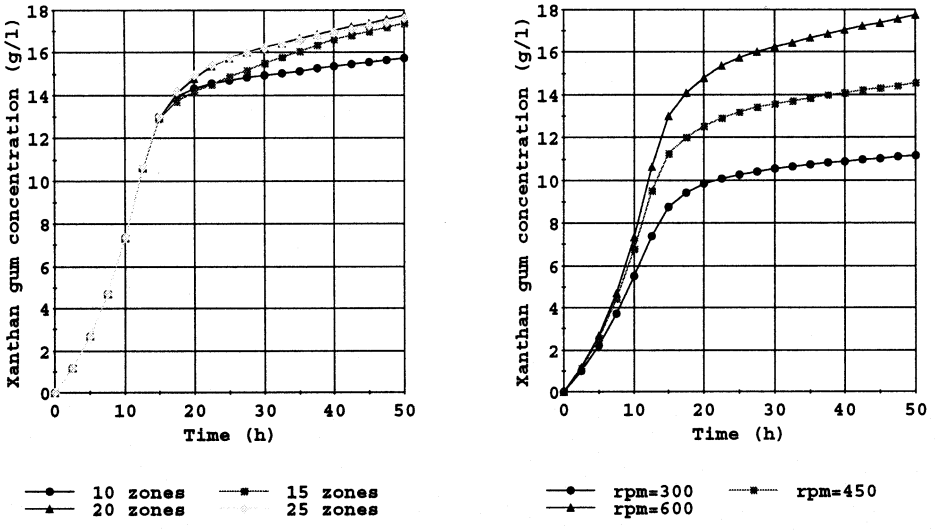

(a) Effect of number of zones at RPM=600

(b) Effect of vessel agitation speed

Figure 5. Variation of predicted xanthan gum concentration over batch duration.

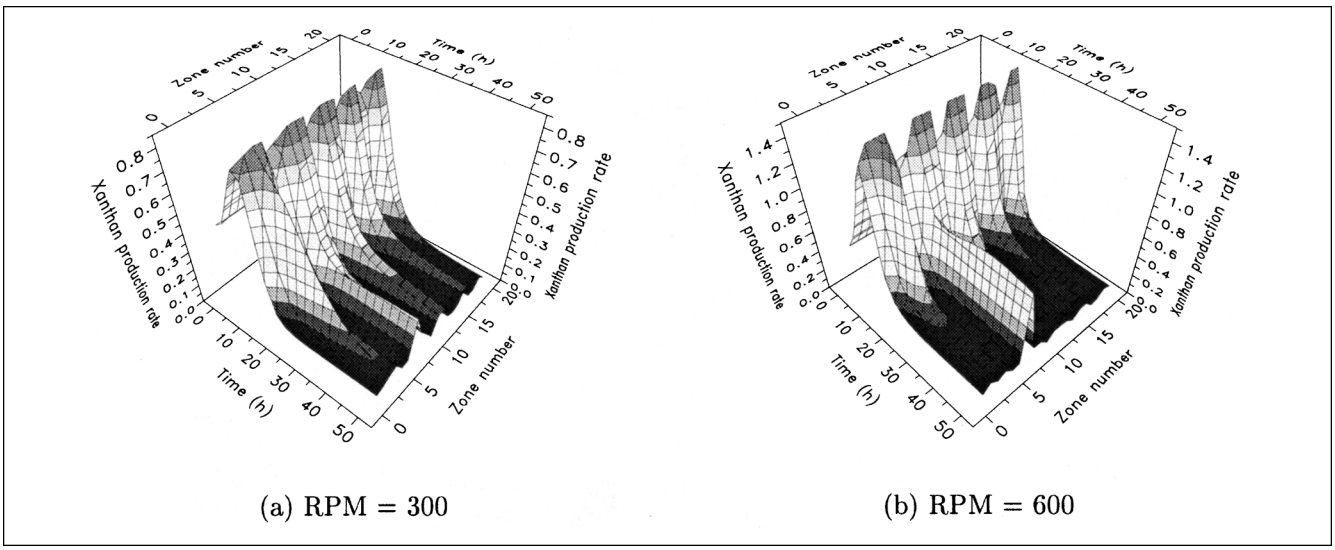

Figure 6. Temporal and spatial variation of xanthan gum production rate (in g/L·h).

A clearer impression of the local variations of critical properties can be obtained by focusing on the three zones shown in Figure 7. Zone 1 is situated between baffles in the top part of the tank, zone 2 is a region under the lower impeller at the bottom of the tank, and zone 3 is the lower impeller region. Figures 8a and 8b show the temporal variation of the xanthan production rate and the viscosity, respectively, in these three zones. In all three regions, the production rate undergoes an initial surge, followed by a sudden drop (at around $t = 10$ h from the start of the batch). In the region near the impeller, the production rate remains at a relatively high level throughout the rest of the batch. On the other hand, near the tank bottom and, even worse, in the poorly mixed region between the baffles and close to the tank wall, the rate steadily decreases to a nearly zero value because of the corresponding increase in viscosity.

Comparison with a perfectly mixed tank model

A much simpler alternative to the hybrid multizonal/CFD model would be a dynamic model based on the assumption that the bioreactor is a perfectly mixed tank (as commonly stated in the literature). It is therefore instructive to compare the predictions of these two models.

For the purposes of the perfectly stirred tank model, the shear rate, S, appearing in the viscosity equation (Eq. 6) is assumed to be directly proportional to the impeller rotation speed (Metzner and Otto, 1957)

$$S = aN, \tag{11}$$

where the proportionality constant, a, has a value of 11.5 (García-Ochoa et al., 2000). All other equations remain the same. The model is fully implemented within gPROMS without any CFD calculations.

Figure 9 compares the temporal variation of the xanthan gum concentration predicted by the two models at two different agitation speeds. It can be seen that, at the start of the batch, the predictions of the two models are very similar. However, as the viscosity of the broth increases, the results start diverging, with the perfectly mixed tank model predicting much higher final xanthan gum concentrations than the hybrid model. In the latter, some regions reach a very high viscosity, which prevents significant mass transfer between the gas phase and the cells. Only regions close to the impeller remain productive; the remaining zones of the reactor soon become a very viscous broth with little reaction taking place.

In conclusion, Eq. 11 allows the perfectly mixed tank model to take limited account of the effects of the agitation speed on the fluid strain, and therefore the viscosity. However, the model fails to account for the reverse effect that the viscosity has on the strain as the concentration of xanthan increases during the batch. Overall, simple models fail to grasp the complex interactions between mixing power, rheology, and fermentation kinetics.

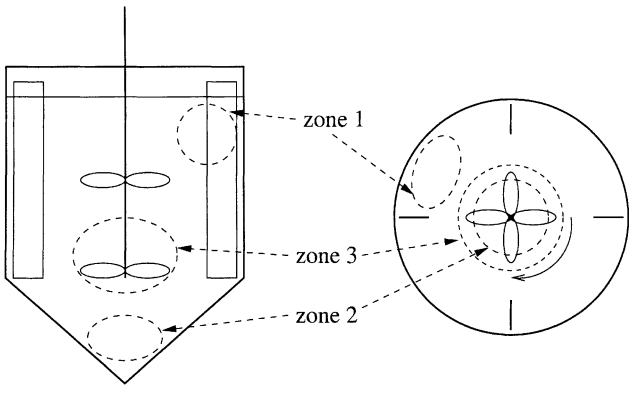

Figure 7. Position of zones used for comparisons in Figure 8.

Use a time-varying agitation speed during batch

The simulation results reported earlier in this section indicate that high rotation speed may improve xanthan gum yield

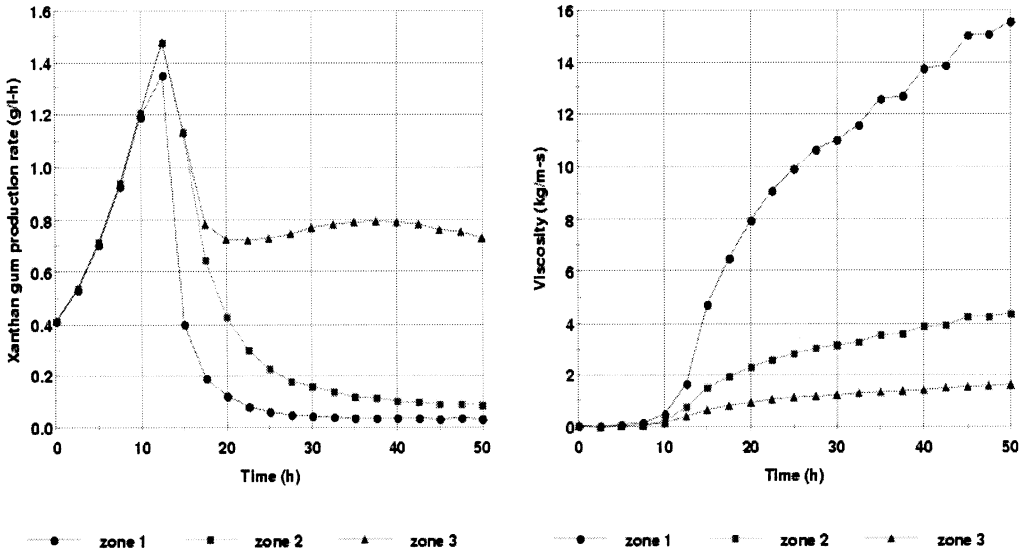

(a) Xanthan production rate (b) Effective viscosity

Figure 8. Differences in temporal behavior in three different zones of the tank at rpm = 600.

in the batch reactor. In practice, very high rotation speeds are inadvisable at the beginning of the fermentation, since they may result in cell damage (García-Ochoa et al., 2000). However, as the broth viscosity increases, the cells of *X. campestris* appear to become less sensitive to shear, probably because of a protective viscous layer of broth that gradually forms around them (Peters et al., 1989). Consequently, fermentation batches are usually started with a relatively low impeller rotation speed of about 200–300 rpm, which is then gradually increased to 700–1,200 rpm (García-Ochoa et al., 1998; Serrano-Carreón et al., 1998).

In view of the preceding considerations, we extend our hybrid multizonal/CFD model to vary the impeller rotation speed during the batch, depending on the volume-average effective viscosity $\overline{\eta}$ given by

$$\overline{\eta} = \frac{\sum_{z=1}^{nz} \eta_z V_z}{\sum_{z=1}^{nz} V_z} \tag{12}$$

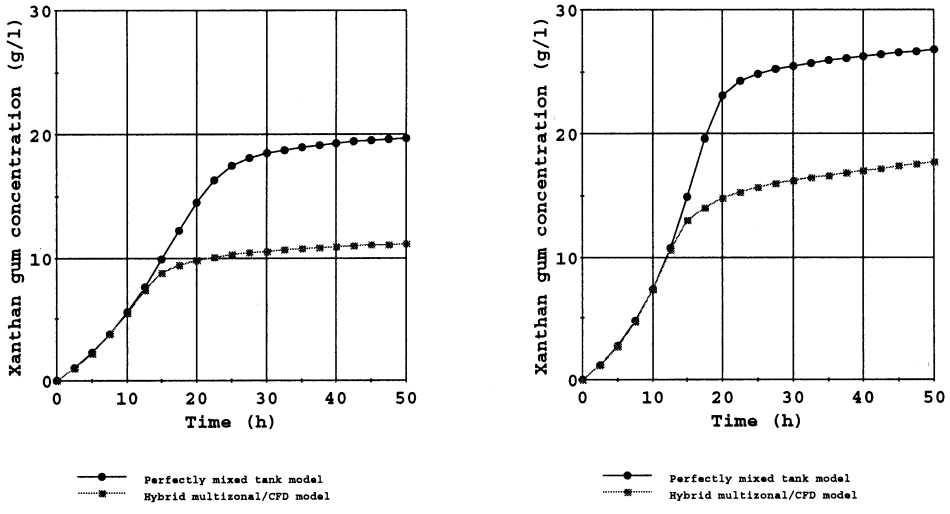

(a) RPM = 300 (b) RPM = 600

Figure 9. Comparison of xanthan gum concentrations predicted by hybrid multizonal/CFD and perfectly mixed tank models.

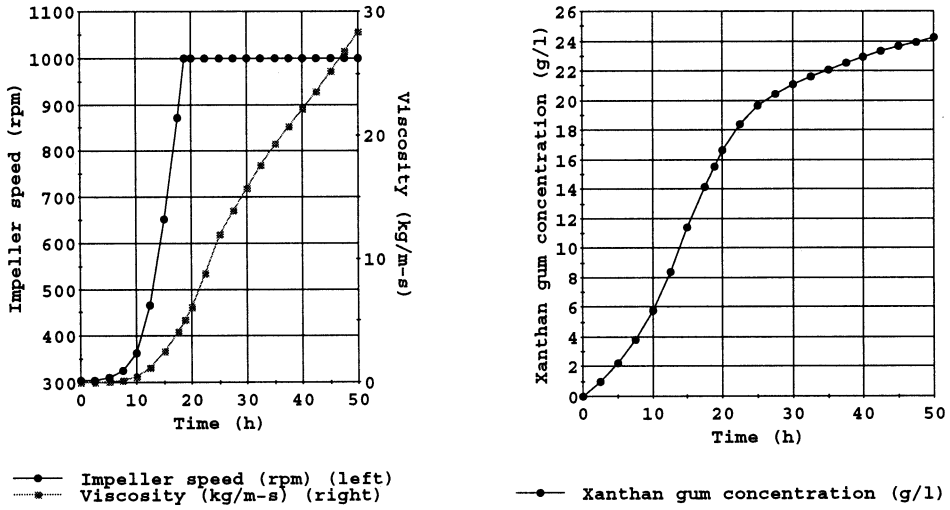

(a) Viscosity and agitation speed (b) Xanthan gum concentration

Figure 10. Xanthan gum production with time-varying agitation speed.

in accordance with the following control law

$$N = \min\left(N_{\max}, N_{\min} + (N_{\max} - N_{\min}), \frac{\overline{\eta}}{\overline{\eta}^*} \right) \qquad (13)$$

where $N_{\min} = 300$ rpm, $N_{\max} = 1{,}000$ rpm, and $\overline{\eta}^* = 5$ kg/m·s.

As illustrated in Figure 10a, the control law just discussed increases the impeller speed from (effectively) 300 rpm until it reaches 1,000 rpm, which occurs when the volume-average viscosity $\overline{\eta}$ reaches the specified critical value $\overline{\eta}^*$, about 20 h from the start of the batch. Thereafter, the agitation speed is kept constant at 1,000 rpm until the end of the batch.

Figure 10b shows that the increasing agitation allows the xanthan gum concentration to keep growing until the end of the batch. The effects of high final agitation are also shown well in Figure 11. Several zones maintain a high productivity right up to the end of the batch, although the agitation is not sufficient to maintain a reasonable production rate in the whole domain. Some zones exhibiting an initial intense xanthan production suddenly fall into ineffectiveness because of varying fluid-dynamic conditions. The behavior of the effective viscosity within the tank (Figure 11b) demonstrates the fact that some regions within the reactors move toward complete immobility, while others maintain a reasonably low viscosity.

Unfortunately, comparisons with experimental data in the literature (for example, García-Ochoa et al., 1998; Serrano-Carreón et al., 1998) are not currently possible due to the lack of detailed information regarding the hydrodynamic and mixing operating conditions under which the various experiments were carried out. Nevertheless, the simulation examples presented in this section demonstrate the unique capability of the hybrid multizonal/CFD model to qualitatively capture the most important phenomena occurring in the xanthan gum production process.

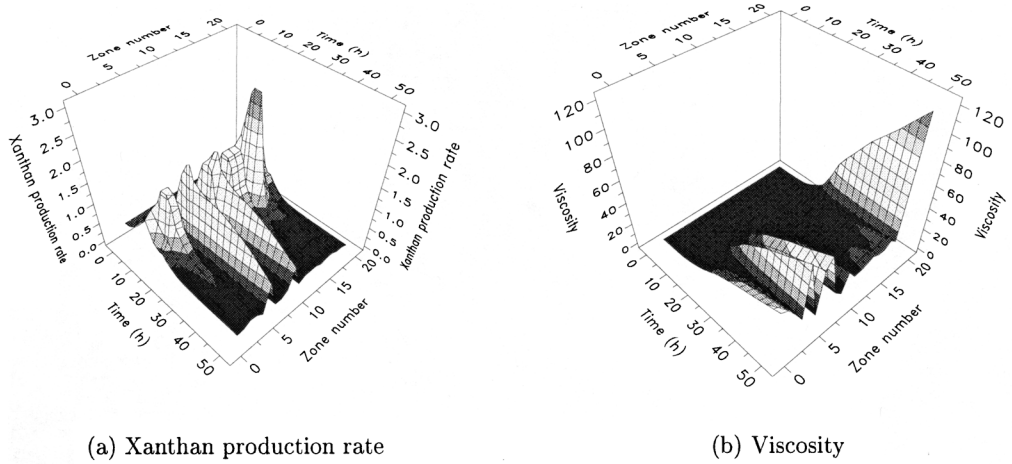

(a) Xanthan production rate (b) Viscosity

Figure 11. Temporal and spatial variations within bioreactor with time-varying agitation speed.

Bioreactor Modeling Using Zone Models Based on Population Balance Equations

The bioreactor models considered earlier in this article have treated the bacteria population as a uniform biomass, that is, a single species being produced according to certain reaction kinetics. In this section, we examine how the hybrid multizonal/CFD modeling approach can be applied to a more detailed description that considers a distribution of cell masses, m. The practical feasibility of such descriptions and their usefulness in handling complex biosystems have been demonstrated in several recent articles in the literature. For example, Zhu et al. (2000) and Godin et al. (1999) have used cell population-balance models to deal with biological systems exhibiting oscillating or periodic behavior. Most of these models are based on work that first appeared in the 1960s and early 1970s, and in particular on the fundamental article by Eakman et al. (1966), which defined the general equations for the description of a population of cells in a mixed vessel.

The population balance–based zone description

The population-balance equation for a particular perfectly mixed zone can be written as (in the interests of clarity, we omit the zone subscript z from the various symbols appearing in this section):

$$V\frac{\partial W(m,t)}{\partial t}+V\frac{\partial}{\partial m}[r(m,t)W(m,t)]$$
$$=2V\int_m^\infty \Gamma(m',t)P(m,m')W(m',t)\,dm'-V\Gamma(m,t)W(m,t)$$
$$+\frac{1}{\rho}\sum_{p=1}^{np}F_p^{\text{in}}W_p^{\text{in}}(m,t)-\frac{1}{\rho}\left(\sum_{p=1}^{np}F_p\right)W(m,t),\quad \forall m>0$$
$$t\geq 0,\quad (14)$$

where the population density function $W(m,t)$ is such that $W(m,t)\,dm$ is the number of cells of mass between m and $m+dm$ per unit volume at time t. The rate of growth of cells of mass m is denoted by $r(m,t)$, while $\Gamma(m,t)$ is the rate at which cells of mass m divide to form two smaller cells. The probability that a cell of mass m will divide into two cells of mass m' and $m-m'$, respectively, is denoted by $P(m,m')$. The rate of cell death is assumed to be negligible.

The preceding hyperbolic partial differential equation is subject to the boundary condition

$$W(0,t)=0,\quad \forall t>0 \qquad (15)$$

expressing the fact that there are no cells of zero mass in the system.

The total mass concentration of biomass in the system can be computed as the first moment of the cell-mass distribution $W(m,t)$ via the equation

$$C_X(t)=\int_0^\infty mW(m,t)\,dm \qquad (16)$$

Cell growth takes place at the expense of the substrate, a balance of which yields the equation

$$\frac{dC_S}{dt}=\frac{1}{\rho}\sum_{p=1}^{np}F_p^{\text{in}}C_{Sp}^{\text{in}}-\frac{1}{\rho}\left(\sum_{p=1}^{np}F_p\right)C_S$$
$$-\frac{1}{Y}\int_0^\infty r(m,t)W(m,t)\,dm \quad (17)$$

where Y is a proportionality constant expressing the amount of biomass that is generated from a unit amount of substrate.

The temporal variation of the concentration, C_i, of any other species, i, present within the zone can be described by an equation of the form

$$V\frac{dC_i}{dt}=\frac{1}{\rho}\sum_{p=1}^{np}F_p^{\text{in}}C_{ip}^{\text{in}}-\frac{1}{\rho}\left(\sum_{p=1}^{np}F_p\right)C_i+Vr_i \qquad (18)$$

where r_i denotes the rate of production (or consumption) of species i, which will generally be a function of the various concentrations, including that of the biomass C_X.

Test system characterization

The zone model described in the previous section requires knowledge of a number of functions and parameters pertaining to the particular system of interest. For the purposes of the simulation experiments to be performed in this article, we assume that the rate of growth for a cell of mass m is given by

$$r=\frac{1}{2}\frac{\log 2}{T_d}m\left(1+\frac{\eta_0}{\eta}\right) \qquad (19)$$

where T_d is the average doubling time of the cell population and η_0 is the initial viscosity of the broth. This equation is based on that proposed by Mantzaris et al. (1999) adapted to include the effects of oxygen mass transport, as these are affected by the broth viscosity, η.

The cell division rate Γ is assumed to depend on both the cell mass, m, and the rate of cell growth, r (cf. Eq. 19), and is given by an expression of the form (Mantzaris et al., 1999)

$$\Gamma(m)=\frac{f(m)}{1-\int_0^m f(m')\,dm'}r \qquad (20)$$

where the division probability density function, $f(m)$, is a lefthand-side truncated Gaussian distribution with set mean, μ_f, and standard deviation, σ_f

$$f(m)=\frac{1}{\sqrt{2\pi\sigma_f^2}}\exp\left[-\frac{(m-\mu_f)^2}{2\sigma_f^2}\right] \qquad (21)$$

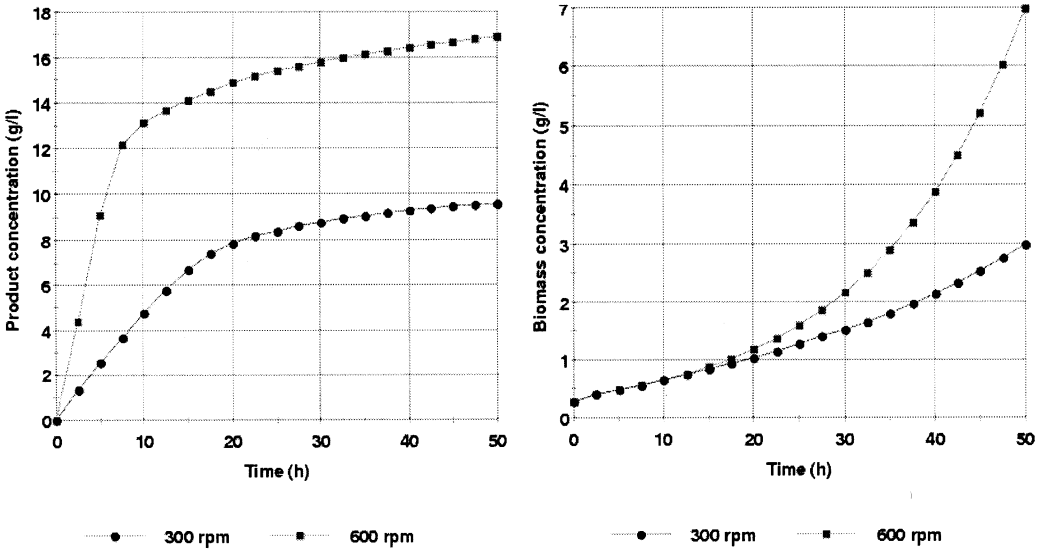

(a) Product (b) Biomass

Figure 12. Effects of agitation speed on volume-averaged product and biomass concentrations in reactor.

The cell partitioning function $P(m,m')$ is assumed to be given by (Mantzaris et al., 1999)

$$P(m,m') = \frac{1}{B(q,q)}\frac{1}{m'}\left(\frac{m}{m'}\right)^{q-1}\left(1-\frac{m}{m'}\right)^{q-1}, \quad \forall m>0$$

$$m' \in (0,m) \quad (22)$$

where q is a preset parameter and $B(q,q)$ is the symmetrical beta distribution defined by the expression

$$B(q,q) = \int_0^1 u^{q-1}(1-u)^{q-1}\,du \quad (23)$$

In addition to the biomass and the substrate, we assume that there are two other species i, namely the product X of the biological reaction and dissolved oxygen O_2, the rates of generation r_i of which (cf. Eq. 18) are given by Eqs. 2 and 4, respectively. The mass transfer of oxygen from the gas to the liquid phase is assumed to be described by Eqs. 5–7.

Several suggestions have appeared in the literature regarding the initial cell-mass distribution, $W(m,0)$ (for example, Subramanian and Ramkrishna, 1971). Here we assume that $W(m,0)$ is a lefthand-side truncated Gaussian (cf. Eq. 21) with a mean of μ_0 and a standard deviation of σ_0.

The values of all new parameters introduced in the population balance model are contained in Table 2.

Table 2. Values of Parameters Used in the Cell Population Balance Model

μ_f	σ_f	μ_0	σ_0	Y	T_d (h)	q
0.575	0.125	0.2875	0.0675	0.5	5	40

Source: Mantzaris et al. (1999).

We note that the preceding combination of functions and parameter values do not necessarily correspond to any particular real system. They are merely intended to be representative choices that will allow us to test the practical feasibility of a hybrid multizonal/CFD model that makes use of population balance-based descriptions for the individual zones.

Simulation results

The integro-partial differential equations presented earlier were discretized using a first-order backward finite difference approximation comprising 50 discretization elements, each of width $\Delta m = 10^{-13}$ g. To improve robustness, the model equations are reformulated in terms of a normalized mass domain 0–1 (corresponding to actual masses of 0 to 5×10^{-12} g) (Mantzaris et al., 1999). Preliminary simulations of well-mixed zones showed that these values allowed adequate accuracy. The discretization resulted in a set of ordinary differential and algebraic equations describing each internal zone in the hybrid model.

Two simulations were carried out at different impeller rotation speeds, rpm = 300 and rpm = 600, respectively. Figure 12 shows the effects of agitation intensity on the volume-averaged concentrations of biomass and product during the batch. The differences in the biomass concentration (computed from Eq. 16) between the two cases demonstrate the effect of mass-transfer variation on the cell growth.

Figure 13 shows the effect of oxygen mass transfer on the growth and distribution of cells. The vertical axis in these figures is the value of $W(m,t)$ volume-averaged across all zones in the hybrid model. Note the different scales of the vertical axes in parts (a) and (b) of this figure. Increasing the impeller speed greatly increases the growth rate and, thus, the biomass in the reactor. Figure 14 shows different projections of the plot in Figure 13a so as to better illustrate the evolution of cell mass during the process.

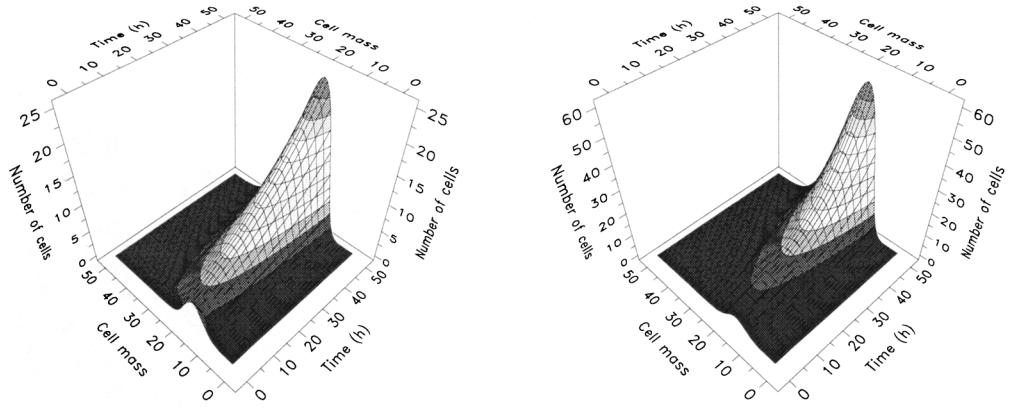

(a) RPM = 300 (b) RPM = 600

Figure 13. Effects of agitation speed on volume-averaged population density function $W(m,t)$ (in number of cells/g·L) for cell masses measured in 10^{-13} g.

The preceding calculations were performed on a SGI Onyx machine (using only one CPU). The simulation took about 8 h, with nearly 80% of the CPU time being consumed by the CFD calculations. Although the computational load is clearly substantial, the deficiencies of a model based on a perfectly mixed tank assumption have already been pointed out in the context of our simpler zone model. On the other hand, it is also worth pointing out that simulating this system via a full CFD calculation would be practically infeasible given the fact that, in view of the discretization of the population density function $W(m,t)$, each and every cell is described by about 55 scalar quantities. Overall, the hybrid multizonal/CFD model appears to offer by far the best trade-off between predictive accuracy and computational complexity.

Concluding Remarks

This article has shown how a general multizonal/CFD modeling methodology can be applied to the study of complex bioreactors operated in batch mode.

From the point of view of modeling of aerobic bioreactors, the description of imperfect mixing afforded by the hybrid model is particularly important because of the nonlinear effects of local viscosity variations on the mass transfer of oxygen from the gas to the liquid phase. Although the use of multizonal (multicompartment) models is well established in these and similar applications, the significant advantage of the hybrid model is that it determines both the flows between adjacent zones and the important hydrodynamic characteristics (such as shear rate) within each zone. On the other hand, the use of "pure" CFD models for studying such bioreactors is practically infeasible: both the modeling of transient operation over many hours and the description of detailed population balances requiring large numbers of quantities in each computational cell of the CFD grid are way beyond the capabilities of present CFD technology.

The hybrid multizonal/CFD modeling approach opens new possibilities in the area of both equipment design (such as in determining optimal equipment geometry, baffle placement, and impeller design) and process operation and control. For

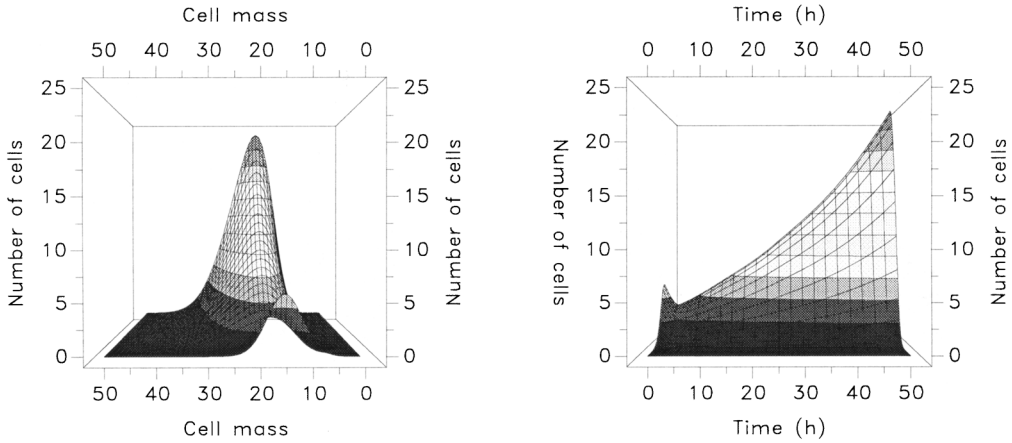

(a) (b)

Figure 14. Distribution of cell mass at rpm = 300-different projections.

example, if more quantitative descriptions of the effects of shear stress (or energy dissipation rate) on cell damage and mass-transfer coefficient were to become available, then it would be possible to derive better strategies for varying agitation speed over the batch duration instead of having to rely on rather simplistic control policies (cf. Eq. 13).

Acknowledgments

The authors thank Fluent Inc., Process Systems Enterprise Ltd., and Bayer AG for the technical support and advice provided during the course of this work. The financial support of the United Kingdom's Engineering and Physical Sciences Research Council (ESPRC) for process modeling research in the Centre for Process Systems Engineering at Imperial College under Platform Grant GR/N08636 is gratefully acknowledged.

Notation

c = cell in CFD model
C_P = xanthan concentration, $(g \cdot L^{-1}) = (kg \cdot m^{-3})$
C_{O_2} = dissolved oxygen concentration, $g \cdot L^{-1}$
$C^*_{O_2}$ = equilibrium dissolved oxygen concentration, $g \cdot L^{-1}$
C_S = substrate concentration, $g \cdot L^{-1}$
C_X = biomass concentration, $g \cdot L^{-1}$
$\mathfrak{C}_z$ = set of CFD model cells that occupy the same space as zone z in multizonal model
F_p, F_p^{in} = outlet/inlet mass flow rate at port p, $kg \cdot s^{-1}$
k = index in the power law model, $Pa \cdot s^n$
$k_L a$ = oxygen mass transfer coefficient, s^{-1}
n = index in the power law model
N = impeller agitation speed, s^{-1}
np = number of ports in a zone
nz = number of zones
p = port in a zone
P = cell partitioning function, $g^{-1} = 10^3 \times kg^{-1}$
V = volume of a zone, $L = 10^{-3} m^3$
V_s = superficial air velocity, $m \cdot s^{-1}$
W = population density function, (no. cells $\cdot g^{-1} L^{-1}$) = ($10^6 \times$ no. cells $\cdot kg^{-1} m^{-3}$)
z = zone in a multizonal model

Greek letters

Γ = cell division rate, $(g^{-1} L^{-1} h^{-1}) = (10^3/3.6 \times kg^{-1} m^{-3} s^{-1})$
η = effective viscosity, $Pa \cdot s$
ρ = density, $g \cdot L^{-1}$

Literature Cited

Al-Rashed, M. H., and A. G. Jones, "CFD Modelling of Gas Liquid Reactive Precipitation," *Chem. Eng. Sci.*, **54**, 4779 (1999).

Atkinson, B., and F. Mavituna, *Biochemical Engineering and Biotechnology Handbook*, Macmillan, Houndmills, UK (1991).

Badino, A. C., Jr., M. C. R. Facciotti, and W. Schmidell, "Volumetric Oxygen Transfer Coefficients (*kLa*) in Batch Cultivations Involving Non-Newtonian Broths," *Biochem. Eng. J.*, **8**, 111 (2001).

Bailey, J. E., and D. F. Ollis, *Biochemical Engineering Fundamentals*, McGraw-Hill, Singapore (1986).

Baldyga, J., and W. Orciuch, "Barium Sulphate Precipitation in a Pipe—An Experimental Study and CFD Modelling," *Chem. Eng. Sci.*, **56**, 2435 (2001).

Bauer, M., and G. Eigenberger, "A Concept for Multi-Scale Modeling of Bubble Columns and Loop Reactors," *Chem. Eng. Sci.*, **54**, 5109 (1999).

Bauer, M., and G. Eigenberger, "Multiscale Modeling of Hydrodynamics, Mass Transfer and Reaction in Bubble Column Reactors," *Chem. Eng. Sci.*, **56**, 1067 (2001).

Bermingham, S. K., A. M. Neumann, H. J. M. Kramer, P. J. T. Verheijen, G. M. van Rosmalen, and J. Grievink, "A Design Procedure and Predictive Models for Solution Crystallisation Processes," *Proc. Conf. Foundations of Computer-Aided Process Design*, AIChE Symp. Ser. 323, M. F. Malone, J. A. Trainham, and B. Carnaham, eds., CACHE-AIChE Publications, New York, p. 250 (2000).

Bezzo, F., *Design of a General Architecture for the Integration of Process Engineering Simulation and Computational Fluid Dynamics*, PhD Thesis, Univ. of London, London (2002).

Bezzo, F., S. Macchietto, and C. C. Pantelides, "A General Framework for the Integration of Computational Fluid Dynamics and Process Simulation," *Comput. Chem. Eng.*, **24**, 653 (2000).

Bezzo, F., S. Macchietto, and C. C. Pantelides, "An Object-Oriented Approach to Hybrid Multizonal/CFD Modelling," PSE2003, Int. Symp. on Process Systems Engineering (2003).

Birtigh, A., G. Lauschke, W. F. Schierholz, D. Beck, C. Maul, N. Gilbert, H. G. Wagner, and C. Y. Werninger, "CFD in Chemical Process Engineering from an Industrial Perspective," *Chem. Ing. Tech.*, **72**, 175 (2000).

Cacik, F., R. G. Dondo, and D. Marques, "Optimal Control of a Batch Bioreactor for the Production of Xanthan Gum," *Comput. Chem. Eng.*, **25**, 409 (2001).

Eakman, J. M., A. G. Fredrickson, and H. M. Tsuchiya, "Statistics and Dynamics of Microbial Cell Populations," *Chem. Eng. Prog.*, **62**, 37 (1966).

Enfors, S. O., M. Jahic, A. Rozkov, B. Xu, M. Hecker, B. Jürgen, T. Krüger, T. Schweder, G. Hamer, D. O'Beirne, N. Noisommit-Rizzi, M. Reuss, L. Boone, C. Hewitt, C. McFarlane, A. Nienow, T. Kovacs, C. Trägårdh, L. Fuchs, J. Revstedt, P. C. Friberg, B. Hjerteger, G. Blomsten, H. Skogman, S. Hjort, F. Hoeks, H. Y. Lin, P. Neubauer, R. van der Lans, K. Luyben, P. Vrabel, and Å. Manelius, "Physiological Responses to Mixing in Large Scale Bioreactors," *J. Biotechnol.*, **85**, 175 (2001).

Ferziger, J. H., and M. Peric, *Computational Methods for Fluid Dynamics*, Springer-Verlag, Berlin (1999).

Fletcher, C. A. J., *Computational Techniques for Fluid Dynamics*, Vol. 1. *Fundamental and General Techniques*, Springer-Verlag, Berlin (1991).

Fluent, *FLUENT 4.5 User's Guide*, Fluent, Inc., Lebanon, NH (1998).

García-Ochoa, F., and E. Gómez, "Mass Transfer Coefficient in Stirred Tank Reactors for Xanthan Gum Solutions," *Biochem. Eng. J.*, **1**, 1 (1998).

García-Ochoa, F., E. Gomez-Castro, and V. E. Santos, "Oxygen Transfer and Uptake Rates During Xanthan Gum Production," *Enzyme Microb. Technol.*, **27**, 680 (2000).

García-Ochoa, F., V. E. Santos, and A. Alcón, "Xanthan Gum Production: An Unstructured Kinetic Model," *Enzyme Microb. Technol.*, **17**, 206 (1995).

García-Ochoa, F., V. E. Santos, and A. Alcón, "Metabolic Structured Model for Xanthan Production," *Enzyme Microb. Technol.*, **23**, 75 (1998).

Godin, F. B., D. G. Cooper, and A. D. Rey, "Development and Solution of a Cell Mass Population Balance Model Applied to the SCF Process," *Chem. Eng. Sci.*, **54**, 565 (1999).

Hewitt, C. J., G. Nebe-Von Caron, B. Axelsson, C. M. McFarlane, and A. W. Nienow, "Studies Related to the Scale-Up of High-Cell-Density *E. coli* Fed-Batch Fermentations Using Multiparameter Flow Cytometry: Effect of a Changing Microenvironment with Respect to Glucose and Dissolved Oxygen Concentration," *Biotechnol. Bioeng.*, **70**, 381 (2000).

Kakhu, A. I., B. R. Keeping, Y. Lu, and C. C. Pantelides, "An Open Software Architecture for Process Modelling and Model-Based Applications," *Proc. Conf. Foundations of Computer-Aided Process Operations*, AIChE Symp. Ser. No. 320, J. Pekny and G. Blau, eds., CACHE-AIChE Publications, New York, p. 518 (1998).

Kramer, H. J. M., S. K. Bermingham, and G. M. van Rosmalen, "Design of Industrial Crystallisers for a Given Product Quality," *J. Cryst. Growth*, **199**, 729 (1999).

Li, G. Q., H. W. Qiu, Z. M. Zheng, Z. L. Cai, and S. Z. Yang, "Effect of Fluid Rheological Properties on Mass Transfer in a Bioreactor," *J. Chem. Technol. Biotechnol.*, **62**, 385 (1995).

Liakopoulou-Kyriakides, M., E. S. Tzanakakis, C. Kiparissidis, L. V. Ekaterianiadou, and D. A. Kyriakidis, "Kinetics of Xanthan Gum Production from Whey by Constructed Strains of *Xanthomonas campestris* in Batch Fermentations," *Chem. Eng. Technol.*, **20**, 354 (1997).

Liu, Z. H., and S. Macchietto, "Model Based Control of a Multipurpose Batch Reactor," *Comput. Chem. Eng.*, **19S**, S477 (1995).

Maggioris, D., A. Goulas, A. H. Alexopoulos, E. G. Chatzi, and C. Kiparissides, "Use of CFD in Prediction of Particle Size Distribution in Suspension Polymer Reactors," *Comput. Chem. Eng.*, **22S**, S315 (1998).

Maggioris, D., A. Goulas, A. H. Alexopoulos, E. G. Chatzi, and C. Kiparissides, "Prediction of Particle Size Distribution in Suspension Polymerization Reactors: Effect of Turbulence Nonhomogeneity," *Chem. Eng. Sci.*, **55**, 4611 (2000).

Mantzaris, N. V., J. J. Liou, P. Daoutidis, and F. Srienc, "Numerical Solution of a Mass Structured Cell Population Balance Model in an Environment of Changing Substrate Concentration," *J. Biotechnol.*, **71**, 157 (1999).

Metzner, A. B., and R. E. Otto, "Agitation of Non-Newtonian Fluids," *AIChE J.*, **1**, 3 (1957).

Nagy, E., M. Neubeck, B. Mayr, and A. Moser, "Simulation of the Effect of Mixing, Scale-Up and pH-Value Regulation During Glutamic Acid Fermentation," *Bioprocess Eng.*, **12**, 231 (1995).

Nienow, A. W., "Mixing: Studies at the University of Birmingham on this Traditional Technology Critical in the Manufacture of New Biological Products," *Food Bioprod. Process*, **78-C**, 145 (2000).

Papoutsakis, E. T., "Fluid-Mechanical Damage of Animal Cells in Bioreactors," *Trends Biotechnol.*, **9**, 427 (1991).

Peters, H. U., H. Herbst, P. G. M. Hesselink, H. Lünsdorf, A. Schumpe, and W. D. Deckwer, "The Influence of Agitation Rate on Xanthan Production by *Xanthomonas campestris*," *Biotechnol. Bioeng.*, **34**, 1393 (1989).

Pons, A., C. G. Dussap, and J. B. Gros, "Modelling *Xanthomonas campestris* Batch Fermentations in Bubble Columns," *Biotechnol. Bioeng.*, **33**, 394 (1989).

Process Systems Enterprise, *gPROMS v2.0 Advanced User Guide*, Process Systems Enterprise Ltd., London (2001).

Reuss, M., D. Debus, and G. Zull, "Rheological Properties of Fermentation Fluids," *Chem. Eng.*, 233 (1982).

Serrano-Carreón, L., R. M. Corona, A. Sánchez, and E. Galindo, "Prediction of Xanthan Fermentation Development by a Model Linking Kinetics, Power Drawn and Mixing," *Proc. Biochem.*, **33**, 133 (1998).

Subramanian, G., and D. Ramkrishna, "On the Solution of Statistical Models of Cell Populations," *Math. Biosci.*, **10**, 1 (1971).

Thomson, N., and D. F. Ollis, "Extracellular Microbial Polysaccharides. II. Evolution of Broth Power-Law Parameters for Xanthan and Pullulan Batch Fermentation," *Biotechnol. Bioeng.*, **22**, 875 (1980).

Urban, Z., and L. Liberis, "Hybrid gPROMS-CFD Modelling of an Industrial Scale Crystalliser with Rigorous Crystal Nucleation and Growth Kinetics and a Full Population Balance," *Proc. Chemputers 1999 Conf.*, Düsseldorf, Germany (1999).

Vlaev, D., R. Mann, V. Lossev, S. V. Vlaev, J. Zahradnik, and P. Seichter, "Macro-Mixing and Streptomyces Fradiae, Modelling Oxygen and Nutrient Segregation in an Industrial Bioreactor," *Chem. Eng. Res. Des.*, **78**, 354 (2000).

Wei, H., and J. Garside, "Application of CFD Modelling to Precipitation Systems," *Chem. Eng. Res. Des.*, **75**, 219 (1997).

Zhao, X. M., A. W. Nienow, S. Chatwin, C. A. Kent, and E. Galindo, "Improving Xanthan Gum Fermentation by Changing Agitators," *Proc. European Mixing Conf.*, p. 227 (1991).

Zhu, G. Y., A. Zamamiri, M. A. Henson, and M. A. Hjortsø, "Model Predictive Control of Continuous Yeast Bioreactors Using Cell Population Balance Models," *Chem. Eng. Sci.*, **55**, 6155 (2000).

Manuscript received Sept. 11, 2002, and revision received Jan. 8, 2003.